Cu-precipitation kinetics in α-Fe from atomistic simulations: Vacancy-trapping effects and Cu-cluster mobility

Frédéric Soisson and Chu-Chun Fu
Service de Recherches de Métallurgie Physique, DMN-SRMP, CEA Saclay, 91191 Gif-sur-Yvette, France
(Received 19 June 2007; published 6 December 2007)

We present Monte Carlo simulations of the first stages of the coherent precipitation of copper in α-Fe. Our method is based on a vacancy mediated diffusion model, which takes into account the dependence of vacancy concentrations and migration barriers on the local atomic environment. These parameters are fitted to *ab initio* data, calculated within the density functional theory. The simulated precipitation kinetics is compared with experimental one. The Fe-Cu system is characterized by a low mutual solubility, which results in the formation of almost pure copper precipitates, and by a large difference between the vacancy formation energy in bcc iron ($\sim$2.1 eV) and metastable bcc copper ($\sim$0.9 eV), which leads to strong trapping of vacancies by the precipitates. As a result, precipitates containing up to several tens of copper atoms can be much more mobile than individual copper atoms. This original result is analyzed with a simple model of cluster diffusion, which suggests that the same behavior could be observed in alloys with similar properties.

DOI: 10.1103/PhysRevB.76.214102 PACS number(s): 81.30.Mh, 66.30.−h, 64.75.+g, 05.10.Ln

I. INTRODUCTION

The copper solubility in α-Fe is small, with a maximum of 1.8 at. % at 850 °C.[1] In supersaturated solid solutions, one observes a precipitation of coherent copper clusters which keep the body-centered-cubic (bcc) structure of the iron matrix for radius up to 2 nm.[2,3] During subsequent growth, precipitates pass through faulted structures (3*R* and 9*R*) and finally reach the perfect face-centered-cubic (fcc) structure of the pure copper.[2,3] This copper precipitation—which can be greatly accelerated under irradiation—has long been suspected to play a role in the hardening and embrittlement of some reactor pressure vessel (RPV) steels. It has motivated many experimental studies on copper precipitation in RPV steels and model alloys, both during thermal ageing or under electron, ion or neutron irradiation.[4]

From a theoretical point of view, the Fe-Cu system has been frequently studied as a benchmark case to test the validity of models of phase transformation kinetics,[5–14] mainly because of its relative simplicity: it is a typical unmixing system, with a large and almost symmetrical miscibility gap and small size effects. The Cu-precipitation kinetics has been modeled either by classical theories of nucleation-growth and coarsening,[5] cluster dynamics (CD) methods,[6–9] or Monte Carlo simulations.[10–15] The small size difference between iron and copper atoms and the full coherency of the copper precipitates make rigid lattice approximations well suited to the problem. Classical theories and CD models are usually based on the assumption that the size of precipitates only changes by emission or absorption of individual solute atoms. However, several kinetic Monte Carlo simulations[10,11,16–20] have suggested that in alloys with unmixing tendency, trapping of vacancies at the precipitate/matrix interfaces or within the precipitates may lead to the diffusion without dissociation of small solute clusters. As a consequence, it could favor the direct coagulation between precipitates and modify the precipitation kinetics.

This phenomenon has indeed been observed in previous Monte Carlo simulations of Fe-Cu alloys.[10,11] In Ref. 11, where the Monte Carlo parameters were estimated with an empirical potential, it has been observed that small clusters up to 2–5 copper atoms could be more mobile than Cu monomers, the mobility then rapidly decreases with the cluster size. However, the mobility of small copper clusters appears to be very dependent on the details of the vacancy diffusion mechanisms, especially on the way the vacancy formation energies and diffusion barriers depend on the local copper distribution. Such information is very difficult to get from experimental measurements. In principle, empirical potentials can be used to obtain it, as in Ref. 11, but they are usually not fitted to alloy diffusion properties. The various available potentials for the Fe-Cu system therefore present significant differences in their migration barriers,[21] and their predictive power remains limited. In recent years, first principles calculations have offered a reliable alternative, thanks to the increasing power of computational facilities.[14,22–24]

The first objective of this work is to use *ab initio* calculations to study the thermodynamic and diffusion properties of Fe-Cu alloys which control the kinetics of copper precipitation, i.e., mainly the vacancy formation energies and migration barriers. Subsequently, we try to reproduce these properties using a diffusion model based on a simple rigid lattice approximation, sufficiently rapid to be used in atomistic kinetic Monte Carlo (AKMC) simulations, in order to follow the precipitation kinetics. The simulated kinetics is compared to that available experimentally. Then, we study the diffusion of copper precipitates. They are found to be much more mobile than expected from previous work, which has a strong effect on the precipitation kinetics.

II. METHODS

A. *Ab initio* calculations

The formation energies of stable Fe-Cu configurations, as well as the migration barriers, are computed in the frame of the density functional theory (DFT), with the generalized gradient approximation, using the SIESTA code.[25] The

pseudopotential and the basis set for Fe atoms are the same as in Ref. 26. The cutoff radius for the pseudopotential of Cu is set to 1.16 Å for s, p, and d orbitals and to 0.42 Å for the partial core correction. Its basis set consists of two localized functions for the $4s$ states and five for the $3d$ states. The cutoff radii are 2.85 Å. Three functions for the $3p$ states are included as polarized orbitals in order to increase angular flexibility.

The calculations used to get the AKMC parameters have been performed at constant volume, with the equilibrium lattice parameter of pure bcc iron. This choice was made by considering that in dilute iron-copper solid solutions and for small coherent copper clusters, the iron matrix must impose a lattice parameter close to that of pure iron. However, some calculations have also been performed at constant pressure, by optimizing also the volume and the shape of the supercell, to assess the effects of the previous assumption. The Methfessel-Paxton scheme for electronic density of states broadening is used with a 0.3 eV width. Most of the calculations have been done in bcc supercells of 54 atomic sites using a $4\times4\times4$ k point grid, and several checks have been carried out using 128 bcc site cells and a $3\times3\times3$ k point grid. The calculations for copper rich fcc configurations have been performed in fcc supercells of 108 sites with a $4\times4\times4$ k point grid.

In a metal A, the following thermodynamic quantities can be computed at 0 K: the vacancy formation energy:

$$E_V^{for}(A) = E[(N-1)A + 1V] - (N-1)E[A], \quad (1)$$

where $E[(N-1)\mathrm{A}+1V]$ is the energy of a supercell containing $(N-1)$ atoms of A and one vacancy V, in the appropriate crystalline structure, and $E[A]=E[NA]/N$ is the energy per A atom in the same structure; the formation energy (or mixing energy) of a substitutional impurity X:

$$E_X^{sol}(A) = E[(N-1)A + 1X] - (N-1)E[A] - E_{ref}[X], \quad (2)$$

where $E[(N-1)A+1X]$ is the energy of a supercell containing $(N-1)$ A atoms and one X atom, $E_{ref}[X]$ the energy of an X atom (which depends on its reference state, for example, bcc or fcc); and the binding energies between X and Y, lying on nth nearest-neighbor sites:

$$E_{XY}^{b(n)}(A) = E[(N-1)A + 1X] + E[(N-1)A + 1Y] - E[NA] - E[(N-2)A + 1X + 1Y], \quad (3)$$

where $E[(N-2)A+1X+1Y]$ is the energy of a supercell containing N sites, $(N-2)$ A atoms, and one X-Y pair.

The vacancy migration barriers are calculated using the drag method: The atomic positions relative to the center of mass are constrained to relax in the hyperplane perpendicular to the vector connecting the initial and final positions.[27,28]

B. Diffusion model

Ab initio calculations are computationally too expensive to provide the energies and migration barriers corresponding to all the possible atomic configurations around a vacancy. AKMC simulations must therefore be based on a simpler model, fitted to DFT results of typical configurations. Here, we used a rigid lattice model (RLM), where the energy of a configuration is computed as a sum of pair interactions $\varepsilon_{XY}^{(n)}$ between X and Y species lying on nth nearest-neighbor sites (X and Y can be Fe or Cu atoms or vacancies). We will see in Sec. III A that in the case of Fe-Cu alloys, first- and second-nearest-neighbor interactions are sufficient.

This diffusion model has been extensively described in previous works.[10–13,16,19] The jump frequency of an atom (A=Fe or Cu) on a vacancy (V) located on a nearest-neighbor site is given by

$$\Gamma_{AV} = \nu_A \exp\left(-\frac{\Delta E_{AV}^{mig}}{k_B T}\right), \quad (4)$$

where k_B is the Boltzmann constant, ν_A an attempt frequency, and ΔE_{AV}^{mig} the activation energy or migration barrier. The latter is the difference between the total energy of the system when A is at the saddle-point position (E_{sys}^{SP}) and when it is at its initial stable position (E_{sys}^{ini}). In a broken bond model, it writes

$$\Delta E_{AV}^{mig} = E_{sys}^{SP} - E_{sys}^{ini} = e_A^{SP} - \sum_{i,n} \varepsilon_{Ai}^{(n)} - \sum_{j,n} \varepsilon_{jV}^{(n)}, \quad (5)$$

where the sums run over all the bonds which are broken around the atom ($\varepsilon_{Ai}^{(n)}$) and the vacancy ($\varepsilon_{jV}^{(n)}$). The latter vacancy-atom pair interactions have to be introduced to obtain a good description of vacancy formation energies (see Refs. 10–14 and Sec. III B below). The e_A^{SP} parameter corresponds to the binding energy of A with the system when it is at the saddle point (SP); it depends on the local atomic distribution of Fe and Cu atoms. We will see in Sec. III B that in order to better fit the migration barriers of the RLM to the *ab initio* data, it has been chosen to write these SP binding energies as the sum of effective pair interactions between the atom at the saddle point and its six nearest neighbors: $e_{\mathrm{Fe}}^{SP}=\Sigma_i \varepsilon_{\mathrm{Fe}i}^{SP}$ and $e_{\mathrm{Cu}}^{SP}=\Sigma_i \varepsilon_{\mathrm{Cu}i}^{SP}$, according to the method previously used with an empirical potential.[11]

C. Monte Carlo simulations

AKMC simulations are performed using a residence time algorithm,[29] periodic boundary conditions, and simulation boxes containing N atomic sites and one vacancy (with $N=64^3$ for precipitation kinetics and smaller box sizes—between $N=8^3$ and $N=32^3$ for the measurements of diffusion coefficients—see Secs. III B and IV C). At each Monte Carlo step (MCS), there are z_1 possible vacancy jumps, where $z_1=8$ is the coordination number. Using a random number, one of them is chosen with a probability proportional to its frequency Γ_i. The physical time associated with the MCS is given by $t_{MCS}=(\Sigma_{i=1,z_1}\Gamma_i)^{-1}$.

In addition to the migration barriers, a key parameter which affects the precipitation kinetics is, of course, the vacancy concentration. Most of the AKMC simulations published to date considered constant vacancy concentrations. However, in real systems, the local vacancy concentrations are determined by the vacancy formation energy, which depends on the solute concentration and distribution. Therefore, the total vacancy concentration evolves with the state of the system.

In our simulation, the ratio between local vacancy concentrations is also controlled by the difference in vacancy formation energies, but the total concentration $(1/N)$ is imposed: the physical time must be rescaled to take this into account. Here, we used the method described in Ref. 11: During the simulation, one computes the vacancy concentration in pure iron $C_V^{MC}(\mathrm{Fe})$, defined as the concentration on sites without Cu atoms among their first and second nearest neighbors. In practice one measures the fraction of time $f_V^t(0)$ spent by the vacancy on such sites, which gives

$$C_V^{MC}(\mathrm{Fe}) = f_V^t(0)\frac{1}{NX_{\mathrm{Fe}}^0}, \tag{6}$$

where X_{Fe}^0 is the volume fraction of pure iron (for dilute alloys, $X_{\mathrm{Fe}}^0 \simeq 1$). Since the true equilibrium concentration in pure iron is $C_V^{eq}(\mathrm{Fe}) = \exp[-E_V^{for}(\mathrm{Fe})/(k_B T)]$, the physical time is rescaled according to

$$t = t_{MCS}\frac{C_V^{MC}(\mathrm{Fe})}{C_V^{eq}(\mathrm{Fe})}. \tag{7}$$

This method provides a reliable time scale: It guarantees, for example, that the copper diffusion coefficient in the iron matrix remains constant during the formation of precipitates (if the variation the solute content in the matrix is negligible), which is not the case with conservative vacancy approximations. However, it should be noticed that the rescaling is based on the assumption that the vacancy concentrations remain at equilibrium during the precipitation, i.e., that the creation and annihilation of vacancies at dislocations, grain boundaries, etc., are much more rapid than the precipitation process. The same assumption is made in the classical theories of nucleation, growth, and coarsening, as well as in CD models.

III. THERMODYNAMICS AND DIFFUSION PROPERTIES OF IRON-COPPER ALLOYS

A. Thermodynamics

1. Ab initio results

Equilibrium lattice parameters of α-Fe (2.88 Å) and stable fcc copper (3.67 Å) computed with the SIESTA are close to the experimental values [2.87 and 3.61 Å (Ref. 30)]. The lattice parameter of bcc copper (2.91 Å) is close to that of α-Fe, which explains why the energies computed at constant volume (with the lattice parameter of pure iron) and at constant pressure are very similar (Table I).

The vacancy formation energy is approximately 2.1 eV in ferromagnetic α-Fe, in good agreement with experimental values[31] and previous *ab initio* calculations.[22,26] It is smaller in fcc copper, 1.3 eV, also in good agreement with experimental results,[31] and even smaller in bcc copper, approximately 0.9 eV. We can then expect a strong vacancy trapping in copper rich coherent precipitates.

We have taken an interest in the properties of both bcc iron rich and bcc copper rich alloys, which correspond, respectively, to the configurations in the iron matrix and in the coherent copper precipitates (Table II). In the first case, the results are quite similar to those already computed by Domain and Becquart with the DFT VASP code.[22] One of the main features of Fe-Cu alloys is a strong tendency to unmixing (or phase separation). The mixing energy of Cu in α-Fe is approximately 0.5 eV (Table II), which explains the low solubility of copper in bcc iron. It is only slightly smaller when the state of reference is bcc (0.48 eV) rather than fcc (0.52 eV) copper, which means that the equilibrium (incoherent) and metastable (coherent) solubility limits should not be very different. The mixing energy of Fe in bcc copper is larger (almost 0.8 eV); iron should then be quite insoluble in copper rich coherent precipitates. The mixing energy of iron in fcc copper is also quite high (0.67 eV)—in agreement with the fact that on the equilibrium phase diagrams, solubility of Fe in copper[32] appears to be smaller than that of Cu in iron.[1]

TABLE I. Vacancy formation and migration energies in pure iron and pure copper, computed at constant pressure (CP) or volume (CV), in supercells of 54, 108, or 128 sites. Comparison with experimental data of Refs. 31 and 36.

	Formation energy (eV)		Migration energy (eV)	
	Expt.	SIESTA	Expt.	SIESTA
Fe bcc	1.80–2.00	2.18 (54 CV)	0.55	0.68 (54 CV)
		2.20 (128 CV)		0.67 (128 CV)
		2.18 (54 CP)		
		2.21 (128 CP)		
Cu fcc	1.28±0.05	1.30 (108 CP)	0.70±0.02	0.64 (108 CV)
		1.31 (108 CP)		
Cu bcc		0.88 (54 CV)		0.30 (128 CV)
		0.79 (128 CV)		
		1.04 (54 CP)		
		0.95 (128 CP)		

TABLE II. Thermodynamic properties in dilute bcc alloys (*ab initio* calculations with 54 sites and relaxation at constant volume).

	Energy (eV)	This study (SIESTA)	Ref. 22 (VASP)
In bcc iron	$E_{\mathrm{Cu}}^{\mathrm{sol}}(\mathrm{Fe})$	0.48[a]	
		0.52[b]	0.50–0.55[b]
	$E_{\mathrm{CuCu}}^{b(1)}(\mathrm{Fe})$	0.15	0.14
	$E_{\mathrm{CuCu}}^{b(2)}(\mathrm{Fe})$	0.03	0.03
	$E_{\mathrm{CuV}}^{b(1)}(\mathrm{Fe})$	0.17	0.17
	$E_{\mathrm{CuV}}^{b(2)}(\mathrm{Fe})$	0.18	0.19
In bcc copper	$E_{\mathrm{Fe}}^{\mathrm{sol}}(\mathrm{Cu})$	0.77	
	$E_{\mathrm{FeFe}}^{b(1)}(\mathrm{Cu})$	0.40	
	$E_{\mathrm{FeFe}}^{b(2)}(\mathrm{Cu})$	0.27	
	$E_{\mathrm{FeV}}^{b(1)}(\mathrm{Cu})$	−0.05	
	$E_{\mathrm{FeV}}^{b(2)}(\mathrm{Cu})$	−0.06	

[a]Reference state bcc Cu.
[b]Reference state fcc Cu.

TABLE III. First- and second-nearest-neighbor pair interactions at 0 K of the rigid lattice model used in the AKMC simulations.

	Pair interactions (eV)
$\varepsilon^{(1)}_{FeFe}$	−0.778
$\varepsilon^{(2)}_{FeFe}$	−0.389
$\varepsilon^{(1)}_{CuCu}$	−0.644
$\varepsilon^{(2)}_{CuCu}$	−0.322
$\varepsilon^{(1)}_{FeCu}$	−0.651
$\varepsilon^{(2)}_{FeCu}$	−0.345
$\varepsilon^{(1)}_{FeV}$	−0.191
$\varepsilon^{(2)}_{FeV}$	−0.095
$\varepsilon^{(1)}_{CuV}$	−0.190
$\varepsilon^{(2)}_{CuV}$	−0.190

This unmixing tendency also results in strong binding energies between solute atoms (Table II). The binding energy between two Cu atoms in α-Fe is high between first nearest neighbors [$E^{b(1)}_{CuCu}(\mathrm{Fe})=+0.15$ eV], lower between second nearest neighbors [$E^{b(2)}_{CuCu}(\mathrm{Fe})=+0.03$ eV], and negligible beyond. The binding energies between Fe atoms in bcc copper are even higher [$E^{b(1)}_{FeFe}(\mathrm{Cu})=+0.40$ eV and $E^{b(2)}_{FeFe}(\mathrm{Cu})=+0.27$ eV]. The binding energies between Cu atoms and vacancy in α-Fe are strong between first- and second-nearest-neighbor sites (respectively, 0.17 and 0.18 eV) and much smaller beyond. Barashev and Arokiam[33] have shown that because of this strong binding up to the second nearest neighbor, the vacancy can turn a copper atom around, without dissociating the CuV pair, which results in a positive coupling between vacancy and copper fluxes. On the other hand, binding energies between vacancies and Fe solute atoms in bcc copper are slightly negative (i.e., repulsive).

2. Rigid lattice model

The pair interactions of the rigid lattice model (Table III) are fitted to *ab initio* data using the following relations:

$$E_V^{for}(A) = -\frac{z_1}{2}\varepsilon^{(1)}_{AA} - \frac{z_2}{2}\varepsilon^{(2)}_{AA} + z_1\varepsilon^{(1)}_{AV} + z_2\varepsilon^{(2)}_{AV}, \tag{8}$$

$$E_B^{sol}(A) = -\frac{z_1}{2}(\varepsilon^{(1)}_{AA} + \varepsilon^{(1)}_{BB} - 2\varepsilon^{(1)}_{AB}) - \frac{z_2}{2}(\varepsilon^{(2)}_{AA} + \varepsilon^{(2)}_{BB} - 2\varepsilon^{(2)}_{AB}), \tag{9}$$

$$E_{XY}^{b(n)}(A) = \varepsilon^{(n)}_{AY} + \varepsilon^{(n)}_{AX} - \varepsilon^{(n)}_{XY} - \varepsilon^{(n)}_{AA}, \tag{10}$$

where $z_1=8$ and $z_2=6$ are the numbers of first and second nearest neighbors. In addition, we have also used the relation

TABLE IV. Comparison between the thermodynamic properties of iron rich and copper rich bcc alloys at 0 K computed with SIESTA and those obtained with the rigid lattice model and the parameters of Table III.

Energy (eV)	SIESTA	RLM
E^{coh}_{Fe}	4.280[a]	4.280
$E^{sol}_{Cu}(\mathrm{Fe})$	0.484	0.545
$E^{b(1)}_{CuCu}(\mathrm{Fe})$	0.150	0.121
$E^{b(2)}_{CuCu}(\mathrm{Fe})$	0.032	0.021
$E^{b(1)}_{CuV}(\mathrm{Fe})$	0.174	0.126
$E^{b(2)}_{CuV}(\mathrm{Fe})$	0.185	0.139
$E^{for}_{V}(\mathrm{Fe})$	2.179	2.179
E^{coh}_{Cu}	3.540[a]	3.540
$E^{sol}_{Fe}(\mathrm{Cu})$	0.768	0.545
$E^{b(1)}_{FeFe}(\mathrm{Cu})$	0.399	0.121
$E^{b(2)}_{FeFe}(\mathrm{Cu})$	0.265	0.021
$E^{b(1)}_{FeV}(\mathrm{Cu})$	−0.063	−0.118
$E^{b(2)}_{FeV}(\mathrm{Cu})$	−0.047	−0.006
$E^{for}_{V}(\mathrm{Cu})$	0.882	0.882

[a]Experimental values.

$$E_A^{coh} = -\frac{z_1}{2}\varepsilon^{(1)}_{AA} - \frac{z_2}{2}\varepsilon^{(2)}_{AA}, \tag{11}$$

with the *experimental* values of the cohesive energies of pure iron and copper, since *ab initio* calculations of cohesive energies are known to be less reliable than those of energy difference between similar configurations. The use of only pair interactions leads to some limitations: For example, properties (9) and (10) of Fe-Cu and Cu-Fe alloys are symmetrical, $E^{sol}_{Cu}(\mathrm{Fe})=E^{sol}_{Fe}(\mathrm{Cu})$ and $E^{b(n)}_{FeFe}(\mathrm{Cu})=E^{b(n)}_{CuCu}(\mathrm{Fe})$, which is not exactly the case according to the *ab initio* calculations

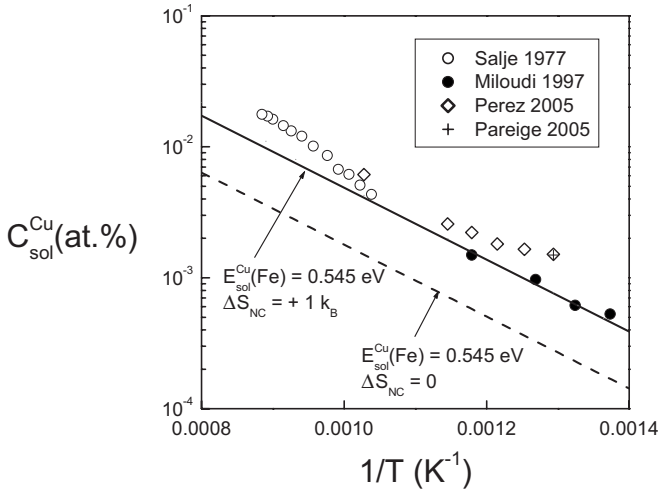

FIG. 1. Copper solubility limit in α-Fe. The symbols correspond to the experimental studies of Salje and Feller-Kniepmeier (Ref. 1), Perez *et al.* (Ref. 52), and Miloudi (Ref. 53) and the lines to Eq. (13) with $\Delta S_{nc}=0$ (dotted line) and $\Delta S_{nc}=1k_B$ (solid line).

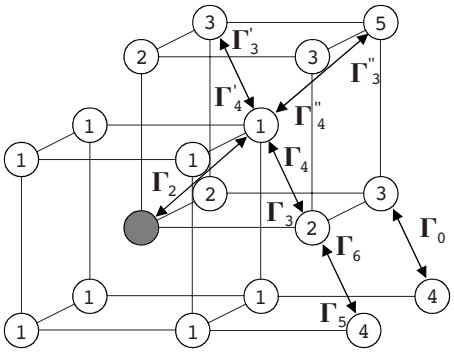

FIG. 2. Vacancy jump frequencies (Γ_i) around a copper atom (gray) and its neighboring iron atoms (white). The arrows indicate the direction of the vacancy jumps; the circled numbers are the order of neighbors to the copper atom.

(Table II). Others relations are imposed, e.g., between mixing and solute-solute binding energies, $E_B^{sol}(A)=4E_{BB}^{b(1)}(A)+3E_{BB}^{b(2)}(A)$, which are not fulfilled according to *ab initio* results, especially for Fe-Fe interactions in bcc copper. Nevertheless, we obtain a reasonable agreement (Table IV) with first- and second-neighbor pair interactions. Since we deal with dilute Fe-Cu alloys, the priority has been the reproduction of the properties of iron rich configurations.

The resulting copper mixing energy in iron (0.545 eV) is slightly larger than the *ab initio* data (0.48 eV). It is close to those used in the AKMC simulations of Schmauder and Binkele (0.515 eV in Ref. 12 and 0.48 eV in Ref. 13) and lower than that used in most of the previous Monte Carlo simulations (0.68 eV in Ref. 10, 0.80 eV in Ref. 11, and 0.83 eV in Ref. 14). In comparison with previous studies, the parameters of Table III also give a larger difference between vacancy formation energies in bcc iron and bcc copper: $E_V^{for}(\mathrm{Fe})-E_V^{for}(\mathrm{Cu})\simeq+1.30$ eV, instead of −0.40 eV in Ref. 10, +0.72 eV in Ref. 11, 0 eV in Ref. 12, and +0.6 eV in Ref. 14.

It has been shown using cluster expansion techniques that it is possible to improve the agreement with *ab initio* calculations by introducing other pair, triangle and tetrahedron effective interactions, in the rigid lattice model.[24] However, taking into account such interactions would slow down the Monte Carlo simulations which are already very time consuming; so here, we restrict ourselves to the pair interactions of Table III. The solubility limit of Cu in iron (as well as that of iron in copper) is then given, at low temperatures, by

$$C_{\mathrm{Cu}}^{sol}(\mathrm{Fe})\simeq\exp\left(-\frac{\Omega}{k_BT}\right), \tag{12}$$

where $\Omega=E_{\mathrm{Cu}}^{sol}(\mathrm{Fe})=E_{\mathrm{Fe}}^{sol}(\mathrm{Cu})$. This approximated value is correct for temperatures well below the critical temperature of the system [$T_c\simeq 0.4\ \Omega/k_B\simeq 2000$ °C (Ref. 34)], which is the case for all the precipitation kinetics considered in this study. The evolution of $C_{\mathrm{Cu}}^{sol}(\mathrm{Fe})$ with the temperature according to several experimental studies is displayed in Fig. 1. We notice some discrepancies among their results. Recent studies, for instance, predict a higher solubility at low temperatures than those expected by extrapolation of the older results measured by Salje and Feller-Kniepmeier[1] at high temperatures.

TABLE V. Migration barriers involved in the impurity diffusion coefficient of Cu in iron, according to Le Claire's diffusion model. Comparison between the results of *ab initio* calculations with SIESTA (this study), VASP (Ref. 21), and the values of the RLM.

	Migration barrier (eV)		
Jump	SIESTA	VASP	RLM
Γ_0	0.68	0.64	0.68
Γ_2	0.59	0.56	0.57
Γ_3	0.64	0.60	0.64
Γ_4	0.64		0.65
Γ_3'	0.70	0.67	0.68
Γ_4'	0.56		0.56
Γ_3''	0.63	0.62	0.68
Γ_4''	0.53		0.56
Γ_5	0.74		0.78
Γ_6	0.55		0.64

With Ω between 0.48 and 0.54 eV, the slope of the Arrhenius plot $\ln C_{\mathrm{Cu}}^{sol}(\mathrm{Fe})=f(1/T)$ predicted by Eq. (12) is in good agreement with the experimental one (Fig. 1), which confirms that the copper mixing energy is indeed in this range. The preexponential factor of Eq. (12), however, gives a slightly too low solubility limit; one can suspect that a nonconfigurational entropy ΔS_{nc} (e.g., a vibration entropy) can explain the discrepancy according to

$$C_{\mathrm{Cu}}^{sol}(\mathrm{Fe})\simeq\exp\left(\frac{\Delta S_{nc}}{k_B}\right)\exp\left(-\frac{E_{\mathrm{Cu}}^{sol}(\mathrm{Fe})}{k_BT}\right). \tag{13}$$

Although such a vibration entropy can be, in principle, computed by *ab initio* methods,[35] we have simply chosen here to fit it directly to the experimental solubility limit; one gets $\Delta S_{nc}=1k_B$ (Fig. 1). In the rigid lattice model, this is done by introducing a small linear variation of the Fe-Cu pair interaction energies: $\varepsilon_{\mathrm{FeCu}}^{(1)}=-0.651-7.83\times10^{-6}T$ and $\varepsilon_{\mathrm{FeCu}}^{(2)}=-0.345-3.92\times10^{-6}T$. The adopted values ($E_{\mathrm{Cu}}^{sol}(\mathrm{Fe})=0.545$ eV and $\Delta S_{nc}=1k_B$) are close to the ones proposed by Christien and Barbu[8] in their CD model [$E_{\mathrm{Cu}}^{sol}(\mathrm{Fe})=0.539$ eV and $\Delta S_{nc}=0.866k_B$] and practically give the same solubility limit.

B. Migration barriers

The *ab initio* calculations of vacancy migration barriers in pure metals give, respectively, 0.67 eV in α-Fe, 0.64 eV in fcc copper, 0.30 eV in bcc copper (Table I). In the two first cases, the values are in rather good agreement with experimental data.[36] The small migration barrier in bcc copper, together with the small vacancy formation energy, should result in a very rapid diffusion in copper rich coherent precipitates.

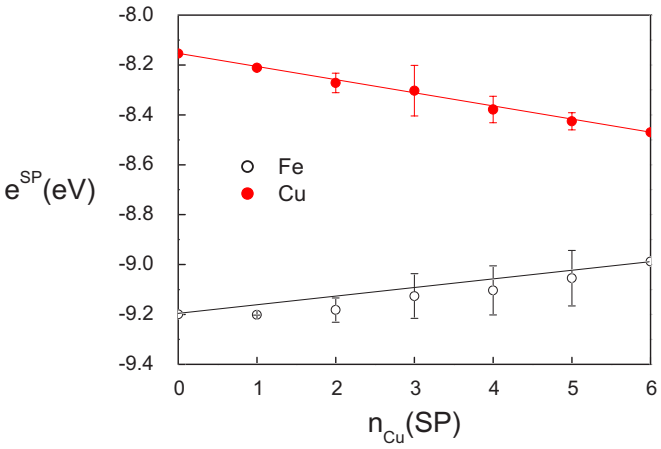

FIG. 3. (Color online) Saddle-point (SP) binding energies of iron and copper atoms as a function of the number of copper atoms among the six nearest neighbors of the saddle point.

The diffusion of Cu in α-Fe plays a key role in the precipitation kinetics; in the classical theories of coherent precipitation, for example, the nucleation, growth, and coarsening rates are proportional to it. We then have computed all the migration barriers which determine the impurity diffusion coefficient of Cu in iron. According to Le Claire's diffusion model,[37] when second-nearest-neighbor interactions are important, ten different jump frequencies must be considered: Γ_0 (Fe-V exchange in pure iron), Γ_2 (Cu-V exchange in pure iron), etc. (the definitions and notations used here are explained in Fig. 2 and in Ref. 11). The migration barriers computed with SIESTA are given in Table V. Our results are very close to the one already published by Becquart and Domain.[21]

TABLE VI. Effective pair interaction energies between atoms at the saddle point and their nearest neighbors.

	Effective SP pair interactions (eV)
$\varepsilon^{SP}_{\mathrm{FeFe}}$	−1.53
$\varepsilon^{SP}_{\mathrm{FeCu}}$	−1.50
$\varepsilon^{SP}_{\mathrm{CuFe}}$	−1.36
$\varepsilon^{SP}_{\mathrm{CuCu}}$	−1.41

In order to study the effect of the local SP configurations, we have also considered Fe-V and Cu-V exchanges in local environments with more than one copper atom and various distributions of Fe and Cu atoms among the six nearest-neighbor positions of the saddle point (20 Cu-V and 20 Fe-V exchanges, in addition to those of Table V). For each barrier, the SP binding energy of the rigid lattice model has been estimated using the pair interaction of Table III and Eq. (5). Figure 3 gives the evolution of Fe and Cu SP binding energies as a function of the number n_{Cu}(SP) of Cu atoms around the SP [the error bars give the dispersion on the barrier for a

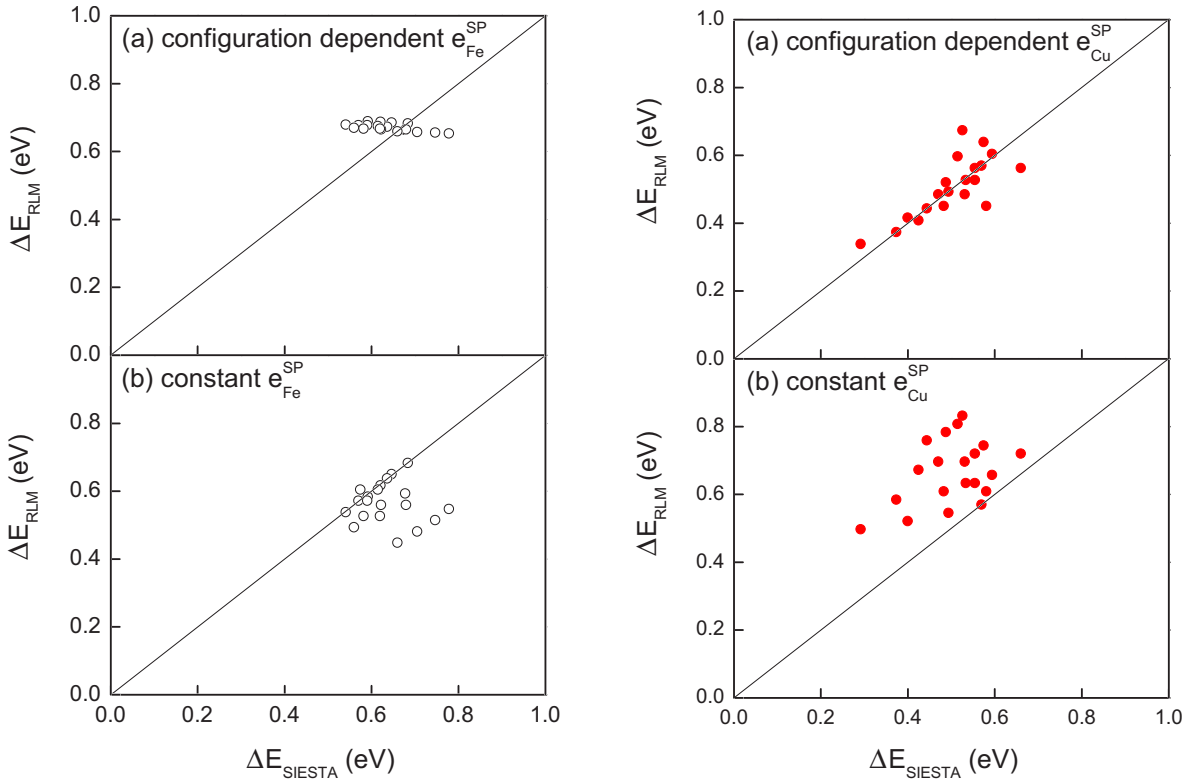

FIG. 4. (Color online) Comparison between the migration barriers of iron (left) and copper (right) computed with SIESTA and with the parameters of the RLM (a) with SP binding energies dependent on the local atomic configuration and (b) with constant SP binding energies.

same value of n_{Cu}(SP) and various distribution among the sites]. It is roughly linear, which suggests that SP binding energies can be written as sums of effective pair interactions between the atom at the saddle point and its six nearest neighbors: $e^{SP}_{Fe}=\Sigma_i \varepsilon^{SP}_{Fei}$ and $e^{SP}_{Cu}=\Sigma_i \varepsilon^{SP}_{Cui}$. A similar result had been previously observed with an empirical potential,[11] but showing a larger variation of the iron SP binding energy. Using the values of Table VI, we finally obtain good agreement between the *ab initio* barriers and the ones of the rigid lattice model (Fig. 4); the mean error on the migration barriers is 0.066 eV for Fe jumps and is 0.039 eV for Cu jump. A simpler model with constant SP binding energies (i.e., with constant e^{SP}_{Fe} and e^{SP}_{Cu} fitted to the *ab initio* barriers in pure iron) would give a slightly less good agreement, especially for Cu-*V* barriers (mean error of 0.072 eV for Fe jump, and 0.162 eV for Cu jumps, see Fig. 4).

To conclude this section, let us stress that due to the time needed for the *ab initio* calculation of migration barriers, the determination of SP binding energies has been done in iron rich configurations; except for the jumping atom, the vacancy, and the first nearest neighbors of the SP position, all the bcc sites were occupied by iron atoms. In future work, migration barriers in copper rich bcc configurations should also be considered in order to improve the description of diffusion in copper clusters.

C. Attempt frequencies

The attempt frequencies ν_{Fe} and ν_{Cu} are fitted to the experimental diffusion data: the self-diffusion coefficient in iron (D_{Fe}) and the copper impurity diffusion coefficients in iron (D_{Cu}) using the Le Claire's diffusion model[37] and the parameters of Tables III and VI. Figure 5 displays the results obtained with $\nu_{Fe}=5\times10^{15}$ s^{-1} and $\nu_{Cu}=2\times10^{15}$ s^{-1}. Because of the lack of experimental data for D_{Cu} at low temperatures, and because of the ferromagnetic transition, which results in a curvature on the Arrhenius plots, this choice calls for the following comments.

(1) For the iron self-diffusion, since available experimental kinetics of precipitation are available in the range 390–550 °C, we have tried to reproduce the diffusion coefficients in the low temperature ferromagnetic phase. Consequently, the iron self-diffusion coefficient of the RLM is in very good agreement with the experimental one below ~600 °C, but too small above this temperature.

(2) For the copper diffusion, above 690 °C, the experimental data show that $D_{Cu}>D_{Fe}$, both in ferromagnetic and paramagnetic iron, with a ratio D_{Cu}/D_{Fe} almost constant (slightly lower than 10). The curvature of the Arrhenius plot makes the extrapolation of D_{Cu} at low temperatures difficult. With the chosen RLM parameters, we keep approximately the same ratio ($D_{Cu}/D_{Fe}\sim10$) in the low temperature ferromagnetic iron.

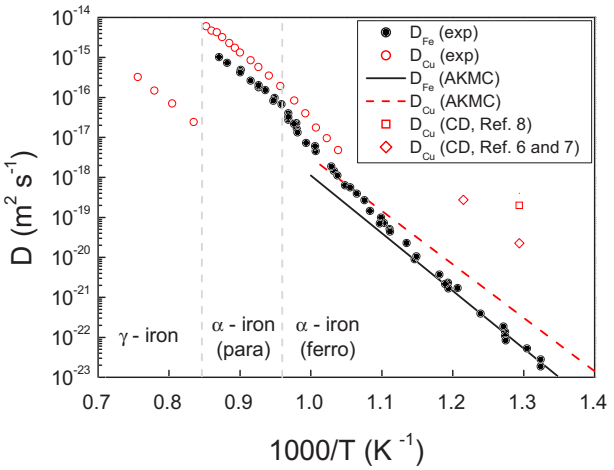

FIG. 5. (Color online) Iron self-diffusion and copper impurity diffusion coefficients. Comparison between the experimental data (Refs. 1 and 36); the coefficients used in our AKMC simulations and the coefficients used in the cluster dynamics modeling of Christien and Barbu (Ref. 8) and Golubov *et al.* (Refs. 6 and 7).

(3) The fitted values of ν_{Fe} and ν_{Cu} are larger than the Debye frequencies by approximately 2 orders of magnitudes. It may mean either that the calculated migration barriers are overestimated with respect to the experimental ones or that other terms (e.g., the vacancy formation entropy) have unusual large values and are indeed included in the attempt frequencies.

IV. Cu-PRECIPITATION KINETICS

In order to validate our model, we first try to compare our results to available experimental kinetics. Then, we deal with the composition of the precipitates, their possible migration, and the effects of such a migration on the precipitation kinetics.

A. Comparison with experimental kinetics

We first consider the precipitation kinetics in a Fe-1.34 at. % Cu alloy, during thermal ageing at 500 °C, which has been extensively studied by atom probe[38,39] or neutron scattering techniques.[40,41] The result of the AKMC simulation is summarized in Fig. 6. In Fig. 6(a), we observe that the fraction of time spent by a vacancy in pure iron decreases dramatically during the copper precipitation, going approximately from 0.4 to 10^{-6}. This evolution is due to the trapping of the vacancy in copper rich clusters. In the initial solid solution, the trapping of vacancies by Cu monomers gives, according to Lomer,[42]

$$f^t_V(0)=\frac{1-z_1C_{Cu}-z_2C_{Cu}}{(1-z_1C_{Cu}-z_2C_{Cu})+z_1C_{Cu}\exp\left(\frac{E^{CuV}_{b1}(Fe)}{k_BT}\right)+z_2C_{Cu}\exp\left(\frac{E^{CuV}_{b2}(Fe)}{k_BT}\right)}, \quad (14)$$

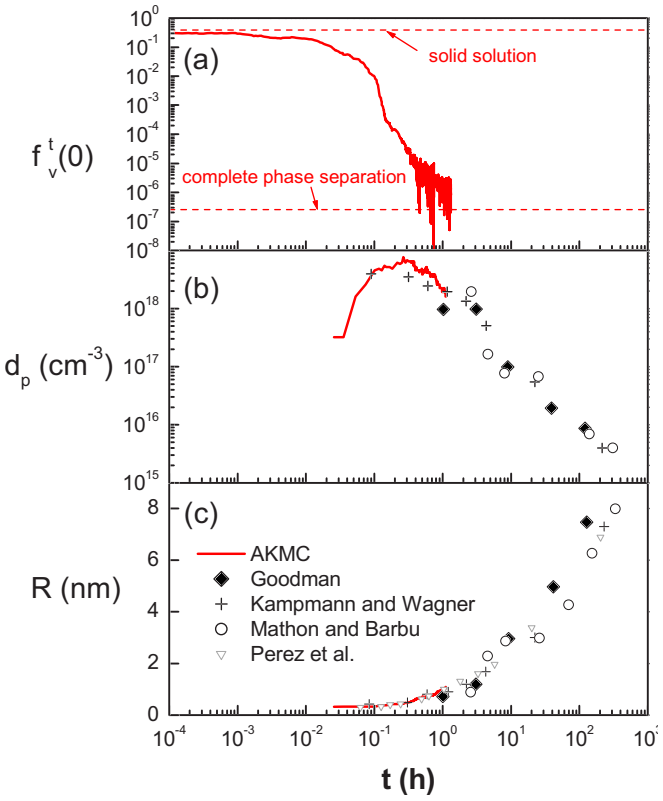

FIG. 6. (Color online) Monte Carlo simulation of the precipitation kinetics in Fe-1.34 at. % Cu during thermal ageing at 550 °C. Evolution of (a) the fraction of time spent by the vacancy in pure iron, (b) the density of precipitates, and (c) the precipitate radius. The solid lines correspond to the simulations and the symbols to experimental studies.

i.e., 0.39 for $C_{\mathrm{Cu}}=0.0134$ and $T=500$ °C. For a complete phase separation between pure Cu and Fe phase and neglecting the interface contribution, we should have

$$f_V^t(0)=\frac{1}{1+\frac{C_{\mathrm{Cu}}}{1-C_{\mathrm{Cu}}}\exp\left(\frac{E_V^{for}(\mathrm{Fe})-E_V^{for}(\mathrm{Cu})}{k_BT}\right)}, \quad (15)$$

which gives 2.54×10^{-7}. For the longer simulation times, this value has not being reached [Fig. 6(a)], which means that the precipitation is not yet complete.

To compute the average density and size of precipitates in the simulations, we only take into account clusters of more than ten copper atoms, connected by at least one nearest-neighbor bond. The exact value of this critical size does not significantly affect the results for time above $t\sim1000$ s—it does not change, in particular, the comparison with experimental results. The trapping effect significantly slows down the Monte Carlo simulations; the mean precipitate radius is slightly above 1 nm after typically a few hundred billions of vacancy jumps, i.e., several weeks of simulations on a standard workstation. We can nevertheless compared the evolution of the number and size of precipitates [Figs. 6(b) and 6(c)] with experimental results; the comparison is limited to the first precipitation steps ($t<10$ h, i.e., to the nucleation and growth regimes and to the very beginning of coarsening) but a good agreement is found between simulations and experiments.

We have also compared our results with electrical resistivity measurements. The experiments of Le *et al.*[43] give the precipitation kinetics at the same alloy composition (Fe-1.34 at. % Cu) for six different temperatures between 390 and 500 °C.

In dilute Fe-Cu alloys, the resistivity is mainly due to solute atoms and small clusters in solid solution.[43] It is then especially useful for the study of the beginning of the precipitation and the growth regime when the solute concentration in the matrix changes the most. If the contribution of a cluster is assumed to be proportional to its interface, the alloy resistivity can be estimated by

$$\rho(t)=\rho_{\mathrm{Fe}}^0+\rho_1\sum_n C_n(t)n^{2/3}, \quad (16)$$

where ρ_{Fe}^0 is the resistivity of pure iron, ρ_1 the resistivity contribution of a copper monomer, and $C_n(t)$ the concentration of copper clusters of size n. The measurement of the size distribution $C_n(t)$ in the simulation therefore gives an estimation of the resistivity, which takes into account the clusters of all sizes (a cluster is again considered as a group of Cu atoms connected by nearest-neighbor bonds). This method has been successfully used by Clouet and Barbu to study the precipitation in Al-Sc alloys.[44] We can then define an advancement factor of the precipitation, $\xi(t)=[\rho(t)-\rho(0)]/[\rho_{\mathrm{Fe}}^0-\rho(0)]$, which can be directly compared to the experimental kinetics.

The advancement factor is found to follow a Johnson-Mehl-Avrami (JMA) law, i.e., $\xi(t)=1-\exp[-(t/\tau)^n]$, with unusually small exponents $n<1$.[10,43] Figure 7 shows that there is an overall good agreement between Monte Carlo simulations and experimental kinetics (for the sake of clarity, only the fit of the experimental data by the JMA law is represented in the figure). The time scale is well predicted by the simulations, except at 390 °C where the AKMC kinetics is 2–3 times more rapid than the experimental ones and at 480 °C where it is slower, especially at the beginning of the precipitation. The time intervals between temperatures are well reproduced.

On the whole, considering that no parameter has been fitted to the precipitation kinetics, we conclude that the predictions of the simulations are reliable.

B. Composition of precipitates

The composition of copper precipitates during thermal ageing has been debated for a long time. The classical theory of nucleation predicts the formation of precipitates with a composition close to the equilibrium one (if the Gibbs-Thompson effect is neglected), i.e., the formation of almost pure copper clusters. However, in their early studies using field ion microscopy (FIM) and atom probe (AP) measurements,[38,39] Goodman *et al.* concluded that precipitates smaller than 5 nm could contain up to 50% of iron. Worrall *et al.*[45] measured a significant but lower iron content ($\sim10\%$) in 3 nm clusters but claimed that the FIM technique could overestimate this proportion by taking into ac-

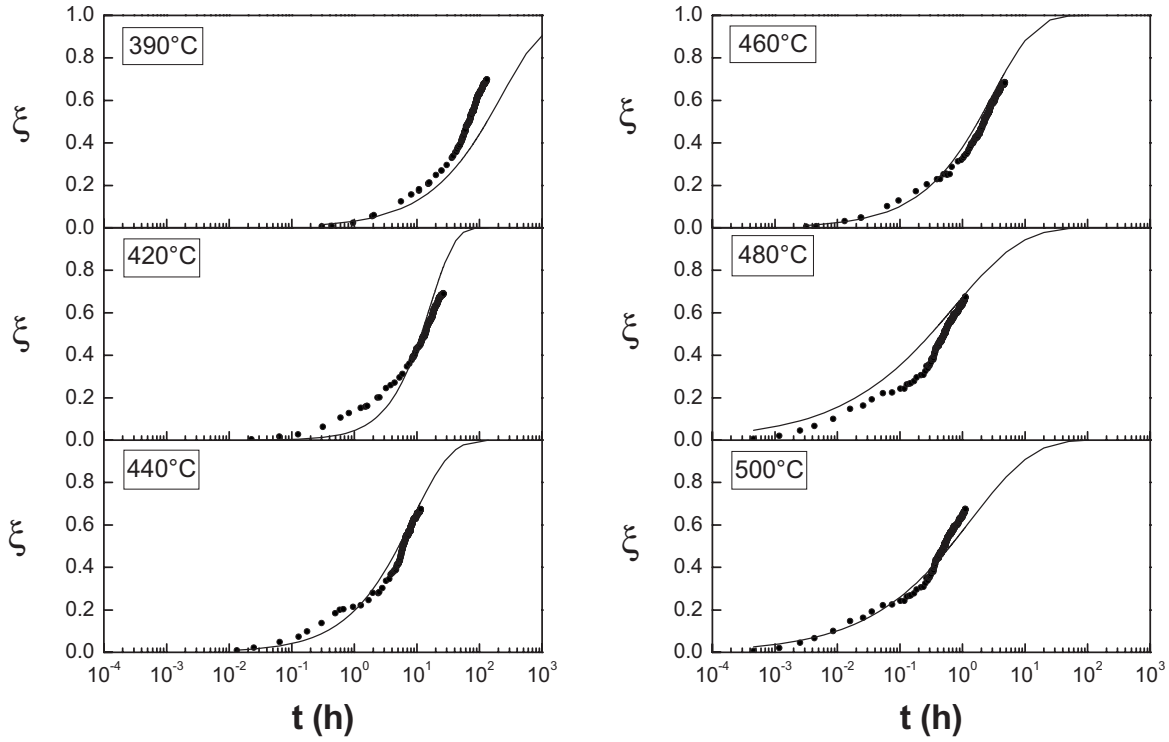

FIG. 7. Evolution of the advancement factor of copper precipitation in Fe-1.34 at. % Cu at six temperatures: electrical resistivity measurements of Le *et al.* (Ref. 43) (lines) and AKMC simulations (black dots).

count a precipitate/matrix interface contribution. Small-angle neutron scattering experiments by Kampmann and Wagner[40] also suggest that precipitates above 1 nm are already pure copper. On the contrary, in a recent three-dimensional AP study of Fe-Cu alloys with significant content of other elements (Ni, Mn, Al, and Si), Isheim *et al.*[46] have observed 1 nm copper rich precipitates with high iron content ($\sim$30 at. %).

In our simulations, copper precipitation in α-Fe clearly occurs by formation of almost pure copper clusters; the concentration profile of a typical precipitate (radius $R \sim 1$ nm) measured by spherical averaging in the simulation, after a thermal ageing of 45 min at 550 °C, is given in Fig. 8. The result is not surprising because of the high mixing energy of iron in bcc copper and the rapid diffusion in bcc copper, which results from both the high vacancy concentration and the low migration barriers. A similar behavior had already been observed in previous AKMC simulations[10,11,14] and appears to be a general trend when the vacancy concentration is higher in the precipitates than in the matrix.[17]

C. Diffusion of copper clusters

The diffusion without dissociation of copper clusters is observed in the Monte Carlo simulations: even the largest precipitates clearly move during the precipitation. The diffusion coefficient of a cluster of n copper atoms can be directly estimated in the AKMC simulation by measuring the mean square displacement of its center of gravity, $\langle R_G^2 \rangle$, according to $D_n = \langle R_G^2 \rangle / 6t$.

In practice, the measurement is only possible using small simulation boxes in a given temperature range (typically between 100 and 350 °C); if the temperature is too high or the boxes too large, solute atoms are emitted, and we measure a diffusion coefficient averaged over the cluster and several monomers. If the temperature is too low, the trapping of vacancies and the correlation effects become so important that the diffusion of a cluster requires too many vacancy jumps, i.e., too much CPU time. In any case, the simulations are long (the present measurements have been done using sequences of $(20-100) \times 10^{10}$ MCSs for each value of D_n) and have been limited to a few cluster sizes.

The results are displayed in Fig. 9; for small copper clusters (below $\sim$150 atoms), the diffusion coefficient of a cluster rapidly increases with its size and then it saturates. At

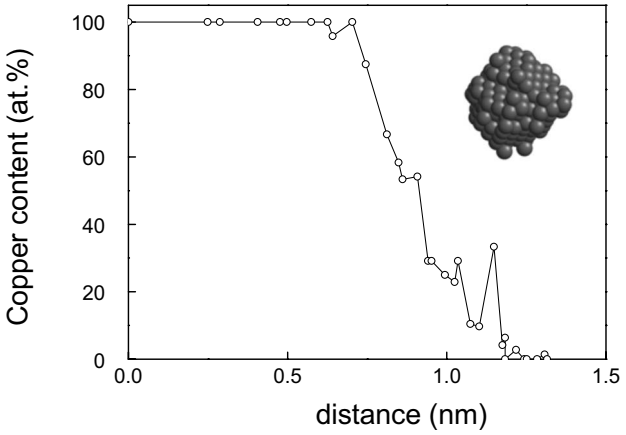

FIG. 8. Concentration profile in a precipitate of 283 copper atoms (Monte Carlo simulation in a Fe-1.34 at. % Cu after a thermal ageing of 45 min at 550 °C).

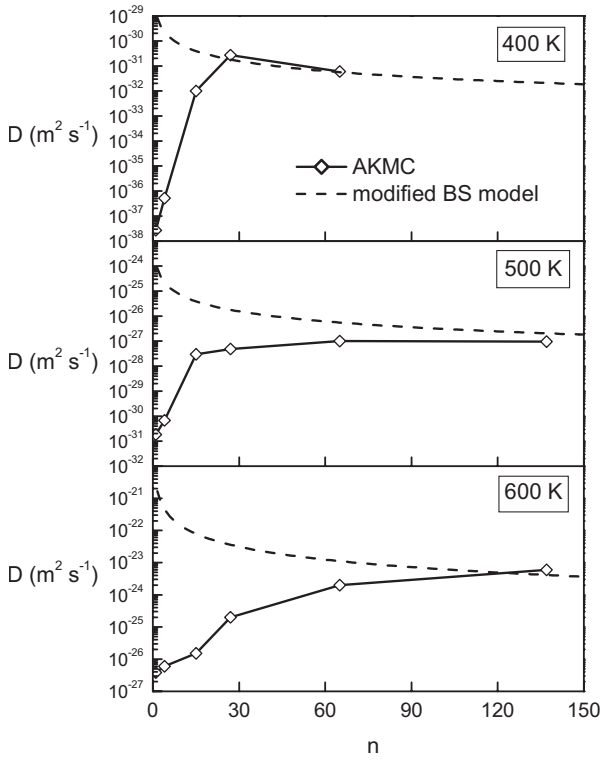

FIG. 9. Diffusion coefficients of clusters of n copper atoms measured by Monte Carlo simulations at 400, 500, and 600 K. The dotted lines correspond to the prediction of the modified Binder-Stauffer (BS) model [Eq. (18)] for large precipitate sizes.

327 °C, for example, a cluster of 137 Cu atoms is approximately 200 times more mobile than a Cu monomer. At 127 °C, the difference is even more spectacular, but the diffusion coefficients are then very small, typically lower than 10^{-30} m^2 s^{-1}. The solute clusters are then much more mobile than in Ref. 11, which was based on an empirical potential and where only the clusters below typically ten atoms were found to be significantly mobile.

The exact analytical calculation of the diffusion coefficient D_n of a cluster of n atoms is a complex problem, especially when diffusion occurs by vacancy jumps. A cluster can adopt several atomic configurations, and many different vacancy jumps can contribute to its displacement, either inside of the cluster or at its interface with the matrix. Moreover, the corresponding atomic jump probabilities strongly depend on the local atomic configuration through the vacancy formation energy and the migration barrier. The computation of the correlation factor for cluster migration is then much more complicated than that of the isolated impurity. Therefore, here we only propose a rougher model to determine the right order of magnitude.

In the context of studies on liquid droplets in a vapor phase, Binder and Stauffer[47,48] and Binder and Kalos[49] have considered the migration of clusters in the case of diffusion by direct exchanges between nearest-neighbor atoms (Kawasaki mechanism). At low temperatures, i.e., for almost pure clusters, the dominant mechanisms occur at the interface: evaporation and/or condensation of atoms or migration along the interface. Without trying to determine the exact nature of the corresponding exchange, they simply consider that when an atom of the cluster jumps over a distance r_s with a frequency Γ_s, the center of gravity of the cluster jumps over r_s/n. Since the number of possible jumps at the interface increases with its area (as $n^{2/3}$), D_n depends on n as

$$D_n \propto \Gamma_s \left(\frac{r_s}{n}\right)^2 n^{2/3}. \tag{17}$$

It should then rapidly decrease with the cluster size (as $n^{-4/3}$) and therefore become negligible by comparison with the monomer diffusion coefficient. At temperatures well below the critical one, the prediction has been checked by Monte Carlo simulations.[49]

When the diffusion mechanism involves point defects, one must take into account their local concentration. In Fe-Cu alloys, the vacancy concentration C_V^{int} at the precipitate/matrix interface is much higher than that in the bulk. To get an order of magnitude, we can estimate the vacancy formation energy at the interface as $E_V^{for}(\text{int}) \simeq [E_V^{for}(\text{Fe}) + E_V^{for}(\text{Cu})]/2$. We have seen that the vacancy concentration is even higher in the copper precipitates, but by analogy with the Binder-Stauffer (BS) model, one may consider that because of the low iron solubility in copper, the corresponding atomic jumps do not contribute to the long range cluster mobility.

The migration barriers at the interface also differ from the ones in the matrix. Therefore, if the cluster diffusion coefficient is controlled by an effective jump frequency Γ_V^{int} at the interface, with an effective migration barrier $\Delta E_V^{mig}(\text{int})$ which takes into account all the jumps which contribute to the cluster migration, D_n is given by

$$\frac{D_n}{D_1} \approx \frac{C_V^{\text{int}}}{C_V^{\text{Cu}}} \frac{\Gamma_V^{\text{int}}}{\Gamma_V^{\text{Cu}}} n^{-4/3}, \tag{18}$$

where $C_V^{\text{Cu}} = \exp\{-[E_V^{for}(\text{Fe}) - E_{b(1)}^{\text{CuV}}(\text{Fe})]/k_B T\}$ is the vacancy concentration on the first-nearest-neighbor sites around a Cu monomer and Γ_V^{Cu} the Cu-V jump frequency in pure iron (i.e., Γ_2 with notation of Sec. III B). With the parameters of Tables III and IV, we get $E_V^{for}(\text{int}) = 1.53$ eV and $C_V^{\text{int}}/C_V^{\text{Cu}} \simeq \exp(+0.524/k_B T)$. This large increase of vacancy concentration (~2600 at 500 °C) is the main effect which explains the high mobility of copper clusters. It also explains the difference with Ref. 11, where the same analysis predicts smaller vacancy enrichment at the interface: $C_V^{\text{int}}/C_V^{\text{Cu}} \simeq \exp(+0.17/k_B T)$. The effective migration barrier at the interface can then be estimated as $\Delta E_V^{mig}(\text{int}) = 0.46$ eV (instead of 0.57 in the bulk) by fitting Eq. (18) on the AKMC measurements (Fig. 9). This lowering of the barriers along the interface is then relevant but much less important than the vacancy-trapping effect, since the corresponding ratio is $\Gamma_V^{\text{int}}/\Gamma_V^{\text{Cu}} = \exp(+0.176/kT) \sim 14$ at 500 °C. We obtain good agreement between Eq. (18) and AKMC measurements for large clusters with well defined interfaces. For small cluster (typically less than 20 atoms), Eq. (18) overestimates the diffusion coefficient because the vacancy trapping is weaker and evolves very abruptly with the size and the detailed structure of the interface.

The high mobility of large copper cluster should favor the direct coagulation between precipitates—as it has been observed in simulations where the vacancy trapping at interfaces was less marked[10,11,17]—and then modify the precipitation kinetics. However, in a previous study, Christien and Barbu have shown that a CD model taking only into account the diffusion of Cu monomers was able to fit the precipitation kinetics of a Fe-1.3 at. % Cu alloy at 500 °C.[8] In their study, the thermodynamic parameters which control the precipitation driving force (mixing energy and entropy of copper in iron) are very close to those used here. On the other hand, the diffusion coefficient of copper in iron they used (2.0×10^{-19} m^2 s^{-1}) is almost 1000 times larger than that of our simulations (3.8×10^{-22} m^2 s^{-1}, see Fig. 5). In another CD model, Golubov *et al.* also used copper diffusion coefficients well above the one of the present work [$D_{Cu}=2.26\times10^{-20}$ m^2 s^{-1} at 500 °C and 2.76×10^{-19} m^2 s^{-1} at 550 °C (Refs. 6 and 7)]. One can suppose that the overestimation of the copper diffusion coefficient compensates the absence of cluster migration.

It would therefore be important to assess what is the real value of D_{Cu} at 550 °C. We have seen that it has not been measured at this relatively low temperature and that extrapolations from higher temperature cannot be very precise (Sec. III C). However, the iron self-diffusion has been measured in the same temperature range, and for "normal" diffusion by a simple vacancy mechanism, one can expect that $0.1<D_{Cu}/D_{Fe}<10$.[50] Our parameters give a D_{Cu}/D_{Fe} ratio slightly below 10, while the values of Refs. 6–8 correspond to D_{Cu}/D_{Fe} between 300 and 1000. Thus, we believe than the values of the present study are more plausible.

V. DISCUSSION AND CONCLUSION

The goal of our study was to model the coherent precipitation kinetics of copper in α-Fe, during thermal ageing, by a coupling between *ab initio* DFT calculations and atomistic kinetic Monte Carlo simulations. To that end, we have considered the properties of Fe-Cu alloys which affect the precipitation kinetic pathways (the vacancy formation energies and migration barriers) and the way they depend on the local iron and copper distribution. Overall, we have found that these properties can be satisfactorily reproduced by a diffusion model of vacancy jumps, with a rigid lattice approximation using:

(i) first- and second-nearest-neighbor pair interactions for the atoms on stable bcc positions to compute the configuration energies;

(ii) first-nearest-neighbor pair interactions for the atoms on saddle-point positions to compute the vacancy migration barrier.

In the AKMC simulations, the estimation of the time scale takes into account the trapping of vacancies in copper rich clusters and the conservation of the equilibrium vacancy concentration in the iron matrix.

One can wonder if it is useful to use such simulation methods which are still computationally expensive, whereas much simpler models—such as cluster dynamics—are available for many years now. Our approach suffers some drawbacks indeed. The restriction to pair interactions only limits the ability of the model to reproduce the *ab initio* calculations, both for thermodynamic properties and migration barriers. In principle, however, it is possible to improve the model by introducing many body effective interactions[24]—at the cost of increase CPU time. The rigid lattice approximation is certainly the most important limitation. Pair interactions are indeed fitted to *ab initio* calculations of relaxed configurations: in this way, the model explicitly takes into account short range elastic interactions. However, long range elastic interactions, which can affect, for example, the shape and distribution of precipitates, are ignored.

Despite these drawbacks, only an atomistic description of diffusion mechanisms can provide the details of phase transformation kinetics without questionable assumptions on the shape or the composition of precipitates, the diffusion of solute complexes, etc. The advantage of *ab initio* calculations is that they give some insight into key properties which control the precipitation kinetic pathways but are very difficult to get from experiments, e.g., properties of metastable bcc copper or migration barriers in alloys. As for the AKMC simulations, they can reproduce the way the vacancy formation energies and migration barriers depend on the local atomic configurations, the correlation effects between successive vacancy jumps, and therefore the whole diffusion properties of solvent and solute atoms. Another strong advantage is that they take precisely into account thermal fluctuations—a key point for nucleation phenomena.

As a result, we have found that AKMC simulations of precipitations in dilute Fe-Cu alloys between 390 and 500 °C are in good agreement with experimental kinetics, even if the comparison is limited to small precipitate sizes (typically 1 nm). We observe the formation of almost pure copper clusters—due to the low solubility of iron and to the high mobility in bcc copper. Thanks to the time rescaling method, the simulations predict an original behavior: the very rapid migration of solute clusters mainly due to vacancy trapping on copper clusters. Precipitates with a few tens of copper atoms are more mobile than individual copper atoms. Since the precipitation occurs in the bulk, it is difficult to check this prediction by direct experimental observations: Coherent copper precipitates are invisible by high resolution transmission electron microscopy[2,3] and the evolution of a sample cannot be followed by atom probe methods. However, kinetic models which only take into account the mobility of copper monomers must overestimate the copper diffusion coefficient; this can be considered as an indirect confirmation of our results.

Finally, a simple model of cluster diffusion has been developed to explain this behavior. It gives the evolution of the cluster diffusion coefficient as a function of its size, in the limit of large cluster sizes (approximately above 100 copper atoms). It depends essentially on the differences in vacancy formation energies and in migration barriers between the matrix and the interface, the first one being dominant in the case of copper precipitation in iron. This model suggests that a significant mobility of solute clusters could be observed in other alloys with similar features. The expression giving the cluster diffusion coefficients could easily be introduced in cluster dynamics[51]—which would allow the modeling of much longer precipitation times.

ACKNOWLEDGMENTS

Fruitful discussions with our colleagues Oliver Rott, Emmanuel Clouet, Maylise Nastar, and Alain Barbu are greatly acknowledged. We thank Julie Tucker for useful reading of the paper. This work is part of the European PERFECT project and supported by the European Commission (FI60-CT-2003-508840).

[1] G. Salje and M. Feller-Kniepmeier, J. Appl. Phys. **48**, 1833 (1977).
[2] P. J. Othen, M. L. Jenkins, and G. D. W. Smith, Philos. Mag. A **70**, 1 (1994).
[3] P. J. Othen, M. L. Jenkins, G. D. W. Smith, and W. J. Phythian, Philos. Mag. Lett. **64**, 383 (1991).
[4] M. H. Mathon, F. Maury, A. Barbu, N. Smetniansky, N. Lorenzelli, C. H. de Novion, and F. Boue, J. Phys. IV **4**, 193 (1994).
[5] A. Deschamps, C. Genevois, M. Nicolas, F. Perrard, and F. Bley, Philos. Mag. **85**, 3091 (2005).
[6] S. I. Golubov, Y. N. Osetsky, A. Serra, and A. V. Barashev, J. Nucl. Mater. **226**, 252 (1995).
[7] S. I. Golubov, A. Serra, Y. N. Osetsky, and A. V. Barashev, J. Nucl. Mater. **277**, 113 (2000).
[8] F. Christien and A. Barbu, J. Nucl. Mater. **324**, 90 (2004).
[9] M. H. Mathon, A. Barbu, F. Dunstetter, F. Maury, N. Lorenzelli, and C. H. de Novion, J. Nucl. Mater. **245**, 224 (1997).
[10] F. Soisson, A. Barbu, and G. Martin, Acta Mater. **44**, 3789 (1996).
[11] Y. Le Bouar and F. Soisson, Phys. Rev. B **65**, 094103 (2002).
[12] S. Schmauder and P. Binkele, Comput. Mater. Sci. **24**, 42 (2002).
[13] P. Binkele and S. Schmauder, Z. Metallkd. **94**, 858 (2003).
[14] E. Vincent, C. S. Becquart, and C. Domain, J. Nucl. Mater. **351**, 88 (2006).
[15] B. D. Wirth and G. R. Odette, in *Phase Transformations and Systems Driven Far From Equilibrium*, edited by E. Ma, P. Bellon, M. Atzmon, and R. Trivedi, MRS Symposia Proceedings No. 481 (Materials Research Society, Pittsburgh, 1998), p. 151.
[16] M. Athenes, P. Bellon, and G. Martin, Acta Mater. **48**, 2675 (2000).
[17] J. M. Roussel and P. Bellon, Phys. Rev. B **63**, 184114 (2001).
[18] P. Fratzl and O. Penrose, Phys. Rev. B **55**, R6101 (1997).
[19] F. Soisson and G. Martin, Phys. Rev. B **62**, 203 (2000).
[20] R. Weinkamer and P. Fratzl, Europhys. Lett. **61**, 261 (2003).
[21] C. S. Becquart and C. Domain, Nucl. Instrum. Methods Phys. Res. B **202**, 44 (2003).
[22] C. Domain and C. S. Becquart, Phys. Rev. B **65**, 024103 (2001).
[23] E. Vincent, C. S. Becquart, and C. Domain, J. Nucl. Mater. **359**, 227 (2006).
[24] F. Soisson and C.-C. Fu, Solid State Phenom. **129**, 31 (2007).
[25] J. M. Soler, E. Artacho, J. D. Gale, A. Garcia, J. Junquera, P. Ordejon, and D. Sanchez-Portal, J. Phys.: Condens. Matter **14**, 2745 (2002).
[26] C. C. Fu, F. Willaime, and P. Ordejon, Phys. Rev. Lett. **92**, 175503 (2004).
[27] C. C. Fu and F. Willaime, Phys. Rev. B **72**, 064117 (2005).
[28] G. Henkelman, G. Jóhannesson, and H. Jónsson, in *Progress on Theoretical Chemistry and Physics*, edited by S. D. Schwartz (Kluwer Academic, Dordrecht, 2000), p. 269.
[29] W. M. Young and E. W. Elcock, Proc. Phys. Soc. London **89**, 735 (1966).
[30] C. Kittel, *Introduction to Solid State Physics* (Wiley, New York, 2005), p. 20.
[31] J. P. Ehrhart, P. Jung, H. Schultz, and H. Ullmaier, in *Atomic Defects in Metals*, edited by H. Ullmaier, Landolt-Börnstein, New Series, Group III, Vol. 25 (Springer, Berlin, 1991).
[32] G. Salje, J. Appl. Phys. **49**, 229 (1978).
[33] A. V. Barashev and A. C. Arokiam, Philos. Mag. Lett. **86**, 321 (2006).
[34] C. Domb, in *Series Expansions for Lattice Models*, edited by C. Domb and M. S. Green (Academic, London, 1974), p. 357.
[35] A. van de Walle and G. Ceder, Rev. Mod. Phys. **74**, 11 (2002).
[36] H. Bakker, H. P. Bonzel, C. M. Bruff, M. A. Dayananda, W. Gust, J. Horváth, I. Kaur, G. V. Kidson, A. D. LeClaire, H. Mehrer, G. E. Murch, G. Neumann, N. Stolica, and N. A. Stolwijk, in *Diffusion in Solid Metals and Alloys*, edited by H. Mehrer, Landolt-Börnstein, New Series, Group III, Vol. 26 (Springer, Berlin, 1990).
[37] A. D. Le Claire, in *Physical Chemistry: An Advanced Treatise*, edited by H. Eyring (Academic, New York, 1970), Vol. 10, p. 261.
[38] S. R. Goodman, S. S. Brenner, and J. R. Low, Metall. Trans. **4**, 2363 (1973).
[39] S. R. Goodman, S. S. Brenner, and J. R. Low, Metall. Trans. **4**, 2371 (1973).
[40] R. Kampmann and R. Wagner, in *Atomic Transport and Defects in Metals by Neutron Scatterings*, edited by C. Janot, W. Petry, D. Richter, and T. Springer (Springer, New York, 1986), p. 73.
[41] M. H. Mathon, A. Barbu, F. Dunstetter, F. Maury, N. Lorenzelli, and C. H. deNovion, J. Nucl. Mater. **245**, 224 (1997).
[42] W. M. Lomer, *Vacancies and Other Point Defects in Metals and Alloys* (Institute of Metals, London, 1958), p. 79.
[43] T. N. Le, A. Barbu, D. Liu, and F. Maury, Scr. Metall. Mater. **26**, 771 (1992).
[44] E. Clouet and A. Barbu, Acta Mater. **55**, 391 (2007).
[45] G. M. Worrall, J. T. Buswell, C. A. English, M. G. Hetherington, and G. D. W. Smith, J. Nucl. Mater. **148**, 107 (1987).
[46] D. Isheim, M. S. Gagliano, M. E. Fine, and D. N. Seidman, Acta Mater. **54**, 841 (2006).
[47] K. Binder and D. Stauffer, J. Stat. Phys. **6**, 49 (1972).
[48] K. Binder and D. Stauffer, Phys. Rev. Lett. **33**, 1006 (1974).
[49] K. Binder and M. H. Kalos, J. Stat. Phys. **22**, 363 (1980).
[50] J. Philibert, *Atom Movements: Diffusion and Mass Transport in Solids* (Editions de Physique, Les Ulis, 1991), p. 161.
[51] P. Mirold and K. Binder, Acta Metall. **25**, 1435 (1977).
[52] M. Perez, F. Perrard, V. Massardier, X. Kleber, A. Deschamps, H. de Monestrol, P. Pareige, and G. Covarel, Philos. Mag. **85**, 2197 (2005).
[53] S. Miloudi, Ph.D. thesis, Université de Paris Sud, 1997.